

Effect of retardation on dynamical mass generation in two-dimensional QED at finite temperature

by

D.J. Lee

Department of Physics
Theoretical Physics
1 Keble Road
Oxford OX1 3NP
U.K.

Abstract

The effect of retardation on dynamical mass generation in *QED* in two space dimensions at finite temperature is studied, in the imaginary time formalism. The photon polarization tensor is evaluated to leading order in $1/N$ (where N is the number of flavours), and simple approximate closed form expressions are found for the fully retarded longitudinal and transverse propagators, which have the correct $T \rightarrow 0$ limit. The resulting Schwinger-Dyson equation for the fermion mass (at order $1/N$) has an infrared divergence associated with the contribution of the transverse photon propagator; only the longitudinal contribution is retained, as in earlier treatments. For solutions in which the mass is a constant, it is found that retardation reduces the value of the parameter r (the ratio of twice the mass to the critical temperature) from about 10 to about 6, in agreement with a similar calculation in the real time formalism. The gap equation is then solved allowing the mass to depend on frequency (but not momentum), thus extending the study of retardation to the variable mass case for the first time. Solutions for $T \neq 0$ are obtained which join on smoothly to the correct $T = 0$ solution. It is found that there is a critical number of flavours, N_c , above which no mass is generated. The phase boundary in the $N - T$ plane is calculated, and agrees qualitatively with that found in other variable mass (but non-retarded) calculations. The r value remains close to 6. Possibilities for including the transverse photon propagator are discussed.

June 1997

1.Introduction

The study of quantum electrodynamics in (2+1) dimensions is of considerable interest, due to its possible relevance to long-wave length models of 2-D condensed matter systems, particularly those which might apply to high T_c superconductors [13], [14]. QED_3 may also give us insight into the phenomenon of dynamical symmetry breaking in theories such as QCD . At zero temperature, a considerable amount of work has been done [1] – [8]. In Appelquist et al [2] it was shown that, using a $1/N$ expansion in the Schwinger-Dyson (S-D) equations, there existed a value $N_c = 32/\pi^2$ above which no fermion mass was dynamically generated, N denoting the number of fermion flavours in the theory. This was found to be qualitatively still true to order $1/N^2$, N_c changing by a factor of $4/3$. [5]. In Pennington and collaborators [3], by contrast, no N_c was found; instead, the dynamically generated mass fell exponentially with increasing N . This work adopted a more general non-perturbative approach to the S-D equations. On the other hand, an alternative non-perturbative study by Atkinson et al [6] claimed that there was indeed a critical number of flavours. More recently, Maris [7] has confirmed the existence of an N_c with a value of about 3.3, more or less independent of the choice of vertex ansatz, by considering the coupled S-D equations for the photon and fermion propagators; and Kondo [8] has studied the problem using the non-local gauge technique.

It is important to extend this type of analysis to finite temperature, because of its possible relevance to physical applications. Here the significant parameters are T_c and r , where r is the ratio of twice the zero temperature fermion mass to the critical temperature, T_c . T_c is the temperature above which chiral symmetry is restored, and at which there is a phase transition from the superconducting phase to the normal phase in the model discussed in [13]. In Dorey and Mavromatos [9] a calculation was done using the S-D equations, with the Matsubara finite-temperature formalism, in which the fermion mass Σ was taken to be constant, and only the Δ_{00} component of the photon propagator was used in the instantaneous approximation—that is, all frequency dependence in the photon propagator was neglected. In this calculation the authors found a value of $r \simeq 10$. If we identify the fermion mass with the order parameter in B.C.S- like theories, this value is much larger than a typical B.C.S value, which is $r \simeq 3.5$. In Aitchison et al [10] the constant mass approximation was relaxed, and instead a momentum -dependent solution

$\Sigma(T, \mathbf{p})$ was calculated. However once again only Δ_{00} in the instantaneous approximation was retained, and it was found that $r \simeq 10$. The r value was therefore insensitive to this refinement in the calculation, although the values of $T_c k_B$ and $\Sigma(T = 0, \mathbf{p} = 0)$ had changed considerably. It was shown in Aitchison and Klein [11] that this value of r also survives the inclusion of a form of wavefunction renormalization. In both the calculations of [10] and [11] the critical value of N was $N_c \sim 2$. It is important to stress that no such N_c existed in the constant Σ case [9].

One obvious problem with the instantaneous approximation in the Matsubara formalism, is that it cannot reproduce the well-studied zero-temperature limit. This is because, as $T \rightarrow 0$, all frequency components should be included, while the instantaneous approximation retains only the $n = 0$ one. To avoid dealing with a large number of frequency components, the first calculation to include retardation in the S-D equations for QED_3 at finite temperature [12] used a real-time formalism, in which the correct $T \rightarrow 0$ was ensured. Making the constant mass approximation, it was found that r was significantly reduced to a value of about 6, from the non-retarded value of about 10.

The calculations of [12], however, did not retain the exact expressions for the longitudinal and transverse photon self-energies, because of their awkward behaviour near zero three-momentum (the amplitudes are non-analytic at the origin, at finite temperature). Instead, a variety of simpler ‘‘average’’ self-energies were used in order to simplify the calculation and to be able to compare the results more easily with those of [9]. In the imaginary time formalism, this difficulty concerning the non-analytic behaviour near zero momentum does not arise, and the exact self-energies can be employed. Our first aim in this paper, therefore, is to include retardation effects, in the constant mass approximation, using the imaginary time formalism. In Section 2 we restate for convenience the results given in [13] for $\Pi_{\mu\nu}$, the photon polarization tensor to leading order in $1/N$. These results involve certain integrals which we first evaluate numerically, and then find simple approximate closed form expressions which retain the correct $T \rightarrow 0$ limit. In section 3 we shall then extend the (constant mass) work done in [9] by using a fully retarded longitudinal propagator. We compare the results with [12], and find rather close agreement.

In section 4 we shall go further and allow the fermion mass to depend

on the (discrete) frequency, still retaining the fully retarded longitudinal self-energy. We believe this is the first time that retardation has been introduced into a “non-constant-mass” S-D calculation at finite temperature. Although we cannot compare our results directly with [10], there are interesting features which remain the same, namely $N_c \sim 2$ and a p_0/α behaviour similar to that of the $|\mathbf{p}|/\alpha$ behaviour of the momentum dependent solution. Our values of $\Sigma(p_0 = 0)$ are found to be in rough agreement with those of $\Sigma(\mathbf{p} = 0)$ in [10]. It would, of course, be interesting to include a dependence of Σ on momentum as well as on frequency, but that is a much harder problem in the retarded than in the instantaneous case.

In section 5 we shall discuss ways of introducing a transverse contribution into our mass-gap equation, which we neglected due to a logarithmic i-r divergence in the zeroth mode. We shall also discuss other possible extensions to our calculation, and we conclude by looking at the plausibility of our calculations in the context of QED_3 as a model of superconductivity.

2. An approximate form for the full photon propagator to leading order in $1/N$

The Lagrangian of massless QED_3 with N flavours is

$$L = -1/4 f_{\mu\nu} f^{\mu\nu} + \sum_i \bar{\psi}_i (i\cancel{\partial} - e\cancel{a})\psi_i \quad (1)$$

where a_μ is the vector potential and $i = 1, 2, \dots, N$. We have also chosen a reducible representation of four-dimensional matrices for the Dirac algebra. Due to the choice of representation eqn (1) has continuous chiral symmetry as discussed in [2].

Following [13] we calculate the full photon propagator in this theory to leading order in $1/N$. We then look for simple closed form expressions to approximate those integrals in the calculation which cannot be evaluated analytically. In these calculations we shall be working in the Landau gauge, in Euclidean space. We first note that the most general photon propagator in the Landau gauge must take the form:

$$\Delta_{\mu\nu} = \frac{A_{\mu\nu}}{p^2 + \Pi_A(p)} + \frac{B_{\mu\nu}}{p^2 + \Pi_B(p)} \quad (2)$$

where $A_{\mu\nu}$ is the longitudinal projection operator and $B_{\mu\nu}$ is the transverse projection operator. To leading order in $1/N$, Π_A and Π_B are the contributions from the loop diagrams shown in fig.1 and are related to the polarization tensor, $\Pi_{\mu\nu}$, at order $1/N$. The projection operators take the following forms:

$$A_{\mu\nu} = \left(\delta_{\mu 0} - \frac{p_\mu p_0}{p^2} \right) \frac{p^2}{\mathbf{p}^2} \left(\delta_{0\nu} - \frac{p_0 p_\nu}{p^2} \right)$$

and $B_{\mu\nu} = \delta_{\mu i} \left(\delta_{ij} - \frac{p_i p_j}{\mathbf{p}^2} \right) \delta_{j\nu}.$ (3)

By using the properties of the projection operators it is easy to show that the inverse propagator must be:

$$\Delta_{\mu\nu}^{-1}(p) = (p^2 + \Pi_A(p))A_{\mu\nu}(p) + (p^2 + \Pi_B(p))B_{\mu\nu}(p). \quad (4)$$

From this expression it is easy to relate $\Pi_{\mu\nu}$ to Π_A and Π_B by summing the diagrams in fig.1 :

$$\Pi_{\mu\nu} = \Pi_A A_{\mu\nu} + \Pi_B B_{\mu\nu}. \quad (5)$$

Then using the explicit forms of $A_{\mu\nu}$ and $B_{\mu\nu}$ in (3) with the additional requirement that $p_\mu \Pi^{\mu\nu} = 0$ one obtains the following forms of Π_A and Π_B :

$$\Pi_A = \Pi_{00} \frac{p^2}{\mathbf{p}^2}$$

$$\Pi_B = \Pi_{ii} - \Pi_{00} \frac{p_0^2}{p^2}. \quad (6)$$

We now proceed with the calculation of $\Pi_{\mu\nu}$ at finite temperature using the Matsubara formalism. We work in imaginary time in which both fermionic and bosonic frequencies are discrete. Fermionic frequencies have the form $p_{0f} = \frac{2\pi}{\beta}(m + 1/2)$ and bosonic frequencies have the form $p_{0b} = \frac{2\pi}{\beta}m$, where m is an integer. From now on we shall denote the modulus of bosonic 3-momenta by p_b and that of fermionic 3-momenta by p_f . In our calculation we need only consider the elements Π_{00} and Π_{ij} . Π_{00} and Π_{ij} are calculated to be [13]:

$$\Pi_{00} = \Pi_3 - \frac{p_{0b}^2}{p_b^2} \Pi_1 - \Pi_2$$

$$\Pi_{ij} = \Pi_1 - \left(\delta_{ij} - \frac{p_i p_j}{p_b^2} \right) + \Pi_2 \delta_{ij} \quad (7)$$

where

$$\begin{aligned}
\Pi_1(p_b, \beta, m) &= \frac{\alpha p_b}{2\pi} \int_0^1 dx \sqrt{x(1-x)} \frac{\sinh(p_b \beta \sqrt{x(1-x)})}{D_m(x, p_b, \beta)} \\
\Pi_2(p_b, \beta, m) &= \frac{\alpha m}{2\beta} \int_0^1 dx (1-2x) \frac{\sin(2xm\pi)}{D_m(x, p_b, \beta)} \\
\Pi_3(p_b, \beta, m) &= \frac{\alpha}{\pi\beta} \int_0^1 dx \ln(4D_m(x, p_b, \beta))
\end{aligned} \tag{8}$$

and

$$D_m(x, p_b, \beta) = \cosh^2(\beta p_b \sqrt{x(1-x)}/2) - \sin^2(xm\pi). \tag{9}$$

m denotes explicit frequency dependence in the above expressions. Using the result

$$\Pi_3 = \Pi_1 + \frac{p_b^2}{p_{0b}^2} \Pi_2 \tag{10}$$

we find that $\Pi_A = \Pi_3, \Pi_B = \Pi_1 + \Pi_2$. Alternatively one can obtain the above expressions for Π_A and Π_B by neglecting Π_2 and setting $\Pi_1 = \Pi_3$, which is found to be a good approximation for Π_{ij} and Π_{00} when $m \neq 0$. For $m = 0$ one can find these expressions without again using eqn (10), by noticing that $\Pi_2(m = 0) = 0$ and $p_{0b} = 0$.

In our treatment of Π_1, Π_2 and Π_3 it will be convenient to consider the $m = 0$ mode separately. For $m = 0$ we need only consider Π_1 and Π_3 , since $\Pi_2(m = 0) = 0$. For $\Pi_3(m = 0)$, which we shall denote by Π_3^0 , an accurate closed form expression has been given in [10], namely

$$\Pi_3^0 = 1/8 \left(\frac{\alpha}{\beta} \right) \left[|\mathbf{p}|\beta + \frac{16 \ln 2}{\pi} \exp \left(-\frac{\pi}{16 \ln 2} |\mathbf{p}|\beta \right) \right]. \tag{11}$$

We are able to find a similar expression for $\Pi_1^0 = \Pi_1(m = 0)$ by noting that

$$\Pi_1^0 = (|\mathbf{p}|) \frac{\partial}{\partial |\mathbf{p}|\beta} \Pi_3^0 \tag{12}$$

which gives, on combining eqn (11) and eqn (12),

$$\Pi_1^0 = \frac{\alpha}{\beta} \left(\frac{|\mathbf{p}|\beta}{8} \right) \left[1 - \exp \left(-\frac{\pi}{16 \ln 2} |\mathbf{p}|\beta \right) \right]. \tag{13}$$

We now evaluate the integrals $\Pi_1(p_b, \beta, m)$, $\Pi_2(p_b, \beta, m)$ and $\Pi_3(p_b, \beta, m)$ for $m \neq 0$. We show the numerical results of these as functions of $p_b\beta$ and m in figs 2a, 2b and 2c. We see that both Π_1 and Π_3 vary little with the explicit frequency index m . Also we are able to show that $0 < \Pi_2 < \left(\frac{2\ln 2}{\pi}\right) \left(\frac{\alpha}{\beta}\right)$. Π_1 and Π_3 are well approximated by

$$\Pi_1 = \Pi_3 \simeq 1/8 \left(\frac{\alpha}{\beta}\right) (p_b\beta) \quad (14)$$

for $m \neq 0$ as figs 3a and 3b show. Since Π_2 is bounded by $\frac{2\ln 2}{\pi} \left(\frac{\alpha}{\beta}\right)$ it is always smaller than Π_1 for $m \neq 0$, since $\Pi_1 \geq \left(\frac{2\pi}{8}\right) \left(\frac{\alpha}{\beta}\right)$, so we shall neglect it in Π_B .

We now have two expressions for the full photon propagator:

$$\begin{aligned} \Delta_{\mu\nu} &\simeq \frac{A_{\mu\nu}}{|\mathbf{p}|^2 + \Pi_3^0(|\mathbf{p}|)} + \frac{B_{\mu\nu}}{|\mathbf{p}|^2 + \Pi_1^0(|\mathbf{p}|)}, \text{ for } p_{0b} = 0 \\ \Delta_{\mu\nu} &\simeq \frac{A_{\mu\nu}}{p_b^2 + \alpha p_b/8} + \frac{B_{\mu\nu}}{p^2 + \alpha p_b/8}, \text{ for } p_{0b} \neq 0. \end{aligned} \quad (15)$$

The structure of our propagator is consistent with the zero temperature result, to order $1/N$: $\Pi_A = \Pi_B = \alpha p/8$. One should note that although in the zero temperature limit the theory is Lorenz invariant, Lorenz invariance is clearly broken at $T \neq 0$, as (15) shows. This is, of course, because a preferred frame of reference is provided by the heat bath.

3 The Schwinger-Dyson equation and its solution for constant Σ

The full Schwinger-Dyson equation for the fermion propagator at non-zero temperature $k_B T = 1/\beta$ is given by

$$S_F^{-1}(p_f) = S_F^{(0)-1}(p_f) - \frac{e}{\beta} \sum_{n=-\infty}^{\infty} \int \frac{d^2 k}{(2\pi)^2} \gamma^\nu S_F(k_f) \Delta_{\mu\nu}(k_f - p_f) \Gamma^\mu(k_f - p_f, k_f). \quad (16)$$

We now truncate eqn (16) by working to leading order in $1/N$, in which case Γ^ν is replaced by its bare value $e\gamma^\nu$ and we use our form for $\Delta_{\mu\nu}$, the full photon propagator, given in (15). As before [9] we neglect wave function

renormalization; we comment further on this in the next section. On taking the trace of eqn (16) we get the following equation for the mass-gap function Σ

$$\Sigma(p_f) = \frac{\alpha}{N\beta} \sum_{n=-\infty}^{\infty} \int \frac{d^2k}{(2\pi)^2} \Delta_{\mu\mu}(k_f - p_f) \frac{\Sigma(k_f)}{k_f^2 + \Sigma^2(k_f)} \quad (17)$$

where

$$\begin{aligned} \Delta_{\mu\mu}(q_b = k_f - p_f) &= \frac{1}{|\mathbf{q}|^2 + \Pi_1^0(|\mathbf{q}|)} + \frac{1}{|\mathbf{q}|^2 + \Pi_3^0(|\mathbf{q}|)}, \text{ for } q_{0b} = 0 \\ \Delta_{\mu\mu}(q_b) &= \frac{2}{q_b^2 + \alpha q_b/8}, \text{ for } q_{0b} \neq 0 \end{aligned} \quad (18)$$

and $\alpha = Ne^2$. Now we make the approximation that Σ is frequency as well as momentum independent. We can then remove a factor of Σ from each side of the equation, and write the argument of $\Delta_{\mu\mu}$ in (17) as $(\frac{2n\pi}{\beta}, \mathbf{k})$. We now do the angular integration, which is trivial. Rearranging terms gives

$$1 = \frac{a}{2N\pi} [S_L(a, s) + S_T(a, s)]. \quad (19)$$

S_T is the transverse contribution which is expressed as:

$$\begin{aligned} S_T(a, s) &= \int_0^\infty x dx \frac{1}{x^2 + \beta^2 \Pi_1^0} \frac{1}{x^2 + \pi^2 + a^2 s^2} \\ &+ \sum_{m=1}^{\infty} \left(\frac{1}{x^2 + (2\pi m)^2 + 0.125a(x^2 + (2\pi m)^2)^{1/2}} \right) \\ &\times \left(\frac{1}{x^2 + (2\pi(m + 1/2))^2 + a^2 s^2} + \frac{1}{x^2 + (2\pi(m - 1/2))^2 + a^2 s^2} \right) \end{aligned} \quad (20)$$

where $x = \beta|\mathbf{k}|$, $a = \alpha\beta$, and $s = \Sigma/\alpha$. S_L is the longitudinal contribution and is exactly the same, except for Π_1^0 being replaced by Π_3^0 . It is now important to notice that the integral for the 0th transverse mode is logarithmically i-r divergent. This can be seen by observing that as $\beta|\mathbf{k}| \rightarrow 0$, $\Pi_1^0 \rightarrow \left(\frac{\alpha}{\beta}\right) \left(\frac{\pi}{128 \ln 2}\right) |\mathbf{k}|^2 \beta^2$. From now on, we shall retain only the longitudinal mode; in our Conclusion we shall discuss ways of including the transverse mode in our calculations.

So we consider the following equation

$$1 = \frac{a}{2\pi N} S_L(a, s). \quad (21)$$

The integral for the $m \neq 0$ modes can be done analytically. We introduce functions of the form:

$$I(d, a, c) = \int_0^\infty \frac{x dx}{(x^2 + d^2) + a(x^2 + d^2)^{1/2}} \frac{1}{x^2 + c^2} \quad (22)$$

Doing the integral on the R.H.S of eqn (22) gives us the following closed form expressions for $I(d, a, c)$.

$$\begin{aligned} I(d, a, c) &= \frac{1}{2(a^2 + c^2 - d^2)} \ln \left(\frac{c^2}{(d+a)^2} \right) \\ &+ \frac{a}{(c^2 - d^2)^{1/2}(a^2 + c^2 - d^2)} \arctan \left(\frac{(c^2 - d^2)^{1/2}}{d} \right). \end{aligned} \quad (23)$$

With the use of these functions we are able to write $S_L(a, s)$ as

$$\begin{aligned} S_L(a, s) &= \sum_{m=1}^{\infty} I(2\pi m, 0.125a, (a^2 s^2 + (2\pi(m + 1/2))^2)^{1/2}) \\ &+ I(2\pi m, 0.125a, (a^2 s^2 + (2\pi(m - 1/2))^2)^{1/2}) \\ &+ \int_0^\infty \frac{x dx}{(x^2 + \Pi_3^0(x)\beta^2)(x^2 + \pi^2 + a^2 s^2)}. \end{aligned} \quad (24)$$

We now solve eqn (21) numerically. We do this by fixing a and N and varying $s = \Sigma/\alpha$ until the R.H.S is equal to unity. We note the value of s for which eqn (21) is satisfied for those values of N and a . We then choose new values of a and N and repeat the process. If eqn (21) is not satisfied for any s at the values of a and N chosen, the only solution to eqn (17) for constant mass is the trivial one $s = 0$. It is important to note that, in these calculations, the infinite sums are evaluated numerically using Mathematica: the convergence is very slow if an attempt is made to truncate them at a (large but) finite number of terms.

In our analysis we also require the zero temperature limit of eqn (21) which is found to be

$$1 = \frac{1}{(2\pi)^2 N} \int_0^\infty \frac{x dx}{(x^2 + s^2)(x + 0.125)} \quad (25)$$

where $x = |\mathbf{k}|/\alpha$. On doing the integration on the R.H.S one obtains the following equation

$$(2\pi)^2 N/2 = \left(1 - \frac{(0.125)^2}{(0.125)^2 + s^2}\right) \frac{\pi}{2s} - \frac{(0.125)}{(0.125)^2 + s^2} \ln\left(\frac{s}{0.125}\right). \quad (26)$$

Now if $s \ll 0.125$ we get the approximate solution $s \simeq 0.25 \exp(-\pi^2 N/4)$, in agreement with [1], remembering that we are including only the longitudinal self-energy, which contributes one half of the total contribution at zero temperature, so that our “ $2N$ ” corresponds to Pisarski’s “ N ”. In fact, we have found that a more accurate fit to the exact numerical solution of (25) is provided by

$$s \simeq 0.25 \exp(-0.96\pi N). \quad (27)$$

With the zero temperature result and our data for $T \neq 0$, we are able to plot solutions of (21) as a function of $1/a = k_B T/\alpha$ for different values of N , as shown in fig.4. It is important to see that unlike previous calculations our zero temperature results join on smoothly to our finite temperature results. This is because we have used a retarded form of the photon propagator with the correct $T \rightarrow 0$ limit, and not the instantaneous form used in [9]. Another thing to note is that the shapes of the solutions as functions of $k_B T/\alpha$ are markedly different from those of [9], [10] and [11]; they seem more to resemble the shape of the B.C.S constant mass-gap solution. We also plot $T_c k_B/\alpha$ against N , in fig.5. $T_c k_B$ falls off exponentially and takes the following form, to very high accuracy:

$$(T_c k_B)/\alpha \simeq 0.081 \exp(-0.96\pi N). \quad (28)$$

From eqn (27) and eqn (28) we can calculate r , where $r = \frac{2\Sigma(T=0)}{T_c k_B}$; we find $r = 6.17$.

In this calculation there is therefore no N_c . The reason for this can be seen as follows. We first note that increasing s and decreasing a (increasing T) causes the R.H.S of eqn (21), $\frac{a}{2\pi N} S_L$, to get smaller. The condition determining N_c is that $\lim_{a \rightarrow \infty} (a S_L) < 2\pi N_c$ for all s , since then eqn (21) can no longer be satisfied, and the only solution to the gap equation is $s = 0$.

Since S_L is a monotonically decreasing function of s we need only show that $\lim_{a \rightarrow \infty} (aS_L(s=0))$ is finite to establish the existence of N_c . But one easily sees from eqn(26) that $\lim_{a \rightarrow \infty} (aS_L(s=0))$ is actually infinite, and so N_c does not exist.

In [9] the instantaneous approximation was used with the constant gap approximation, giving a higher value r , $r \simeq 10$. There is good agreement between our results and those of [12], in which retardation was included in a real time formalism. For example, in [12], using the “best average self-energy” (Π^{R1} in the notation of [12]), s had the value 0.01205 for $N = 2$, corresponding to a value of $s = 0.1225$ from (27) with $N = 1$; and $(k_B T_c)/\alpha$ was 0.0376, corresponding to 0.0397 from (28). These values lead to $r = 6.41$ in [12] as compared to our value of 6.17. The only other difference between our results and those of [12]-not a large one-is that we see very little change of r with N , whereas [12] found a small variation with N .

In the following section we shall look at solutions which are frequency dependent and contain the retarded photon propagator calculated in section 2.

4 The frequency dependent gap equation

In this section we depart from the constant gap approximation, and attempt to solve the retarded Schwinger-Dyson equation (17) allowing the gap function to depend on frequency only. Frequency dependence can be introduced relatively easily into the equation, unlike momentum dependence which leads to a highly non-trivial angular integral of the kernel of our equation, which is unlikely to have an analytic result. The resulting computational complexity has deterred us from including momentum dependence. This is unfortunate, for it would be interesting to compare results calculated with a full retarded

momentum dependent S-D equation with the results of [10]. While this is true, introducing frequency dependence will give us new insight into the nature of the gap, and as in [10] we shall be able to calculate a value of N_c . In the spirit of [10],

we again neglect wavefunction renormalization. It has been pointed out in [3] that wavefunction renormalization should be introduced, but it has

been found in [11] that for a momentum dependent S-D gap equation, there still exists an N_c and r is little affected.

We start our study of the frequency dependent solution at eqns (17) and (18). We shall restrict ourselves again only to the longitudinal mode; this is because the i-r divergence in the tranverse mode is still present, although only in the mode for which $q_{0b} = k_{0f} - p_{0f} = 0$. We see that because Σ is now frequency dependent we can no longer remove a factor of Σ from each side of eqn (17), and $\Delta_{\mu\mu}$ is now dependent on $p_{0f} = \frac{2\pi}{\beta}(n + 1/2)$. But the angular integration is again trivial. On rearrangement we get:

$$s(n) = \frac{a}{2\pi N} S_L^n(a, s) \quad (29)$$

where as before $s = \Sigma/\alpha$ and $a = \alpha\beta$. S_L^n is the frequency dependent longitudinal contribution, expressed as:

$$\begin{aligned} S_L^n(a, s(n)) &= \int_0^\infty x dx \frac{s(n)}{(x^2 + \beta^2 \Pi_3^0)(x^2 + (2\pi(n + 1/2))^2 + a^2 s(n))} \\ &+ \sum_{m \neq n}^\infty \frac{s(m)}{x^2 + (2\pi(m - n))^2 + 0.125a(x^2 + (2\pi(m - n))^2)^{1/2}} \\ &\times \frac{1}{x^2 + (2\pi(m + 1/2))^2 + a^2 s^2(m)} \end{aligned} \quad (30)$$

where $x = \beta|\mathbf{k}|$. The first term represents the $m = n$ mode, where $q_{0b} = 0$. Again it is possible to do the x -integration. Using the functions, $I(d, a, c)$ we are able to express S_L^n as:

$$\begin{aligned} S_L^n(a, s(n)) &= \sum_{m \neq n}^\infty s(m) I(2\pi|m - n|, 0.125a, (a^2 s^2(m) + (\pi(2m + 1))^2)^{1/2}) \\ &+ \int_0^\infty \frac{x dx}{x^2 + \beta^2 \Pi_3^0} \frac{s(n)}{x^2 + (2\pi(n + 1/2))^2 + a^2 s^2(n)} \end{aligned} \quad (31)$$

Eqn (29) represents an infinite system of non-linear coupled integral equations, one for each mode, m . We can reduce the number of equations that need to be considered by the following particle-antiparticle symmetry property,

$$s(m) = s(-m - 1) \quad \text{where } m \geq 0. \quad (32)$$

It is important that the R.H.S of eqn (32) is $s(-m - 1)$ and not $s(-m)$, since $s(m)$ is a fermionic quantity; p_{0f} is related to m by $p_{0f} = \frac{2\pi}{\beta}(m + 1/2)$. Therefore m and $-m - 1$ represent p_{0f} and $-p_{0f}$ respectively. Using eqn (32) it is possible to cast $S_L^m(a, s(n))$ into a final form convenient for numerical calculations:

$$\begin{aligned}
S_L^m(a, s) &= \sum_{m \neq n \geq 0}^{\infty} s(m) [I(2\pi|m - n|, 0.125a, (a^2 s^2(m) + ((\pi(2m + 1))^2)^{1/2}) \\
&+ (I(2\pi|m + n + 1|, 0.125a, (a^2 s^2(m) + ((\pi(2m + 1))^2)^{1/2})] \\
&+ \int_0^{\infty} \frac{x dx s(n)}{(x^2 + \beta^2 \Pi_3^0(x))(x^2 + (\pi(2n + 1))^2 + a^2 s^2(n))} \quad (33) \\
&+ s(n) I(2\pi(2n + 1), 0.125a, (a^2 s^2(n) + ((\pi(2n + 1))^2)^{1/2}),
\end{aligned}$$

the last term being the $n = -m - 1$ mode in eqn (31). Although eqn (33) looks cumbersome compared with eqn (31), the advantage is now that only positive values of n and m need be considered, thereby reducing the number of equations in the system (29).

In our numerical calculation we will want to limit the number of equations to a finite number, M . We can think of eqn (29) as a sort of non-linear matrix problem, where instead of an infinite matrix we will restrict ourselves to an $M \times M$ matrix. The justification for doing this is simple: we expect our solution to fall off monotonically with n , and as $n \rightarrow \infty$ we expect $s(n) \rightarrow 0$. The effective limit M on the matrix size is determined by the requirement that $s(n - 1 = M)$ be one tenth the size of $s(0)$, which is the maximum value of s as a function of n . In choosing this size of matrix, the contribution from modes for which $n - 1 > M$ has a very small effect upon our solution. Note that whereas in the constant mass case (Section 3) we had to include all frequencies in our summations, when the mass is frequency- dependent a natural cut-off emerges.

The method we shall normally adopt (“method I”) in solving the equations (29) will be to start with a trial function having the correct $n \rightarrow \infty$ limit, namely $s(n) \rightarrow 0$. We insert this trial function into eqn(33). Then we

work out the resultant value of $s(n)$ using eqn (29), and reinsert the result back into eqn (33). After several such iterations we check if our matrix size is sufficient, by seeing if $s(n-1) \leq 0.1s(0)$; if it is appreciably larger we increase the size of our matrix. To do this, we increase the value of m at which we truncate the sum in eqn (33), and we increase the number of equations in eqn (29) we must solve. When we are satisfied with the size of our matrix we keep iterating until $s(n)$ changes by less than 1% over ten iterations (or more depending on the rate of convergence to the exact solution). It should be appreciated that the non-linearity of the system of equations requires this further iteration, even after deciding on the size of the matrix.

If the rate of convergence is very slow, which is the case near a phase transition, we use “method II”. In method II we choose two trial functions. One of them, \tilde{s}_\downarrow , is chosen to decrease in magnitude with each iteration using method I; the other, \tilde{s}_\uparrow , to increase in magnitude with each iteration. We then average the two functions together, $s = 0.5(\tilde{s}_\uparrow + \tilde{s}_\downarrow)$. Then we use method I on \tilde{s} for ten iterations or more. If \tilde{s} increases in magnitude we set $\tilde{s}_\uparrow(n) = \tilde{s}(n)$; if \tilde{s} decreases in magnitude we set $\tilde{s}_\downarrow(n) = \tilde{s}(n)$, and we average again. We repeat the process until \tilde{s}_\uparrow and \tilde{s}_\downarrow vary little from each other.

An important technical difficulty is that as T gets smaller the size of our matrix increases: as $T \rightarrow 0, M \rightarrow \infty$, and the larger M is, the slower the calculation of $s(n)$. Fortunately most of the interesting behaviour lies in a region of temperature where the matrix size, M , is manageable. Although we cannot approach close to the $T \rightarrow 0$ limit from our finite temperature calculations, we can get around this difficulty by including an analytic $T \rightarrow 0$ limit to eqn (28),

$$s\left(\frac{p_{0f}}{\alpha}\right) = \frac{1}{(2\pi)^2 N} \int_0^\infty dy s(y) \left(I\left(y - \frac{p_{0f}}{\alpha}, 1/8, \sqrt{y^2 + s(y)}\right) + I\left(y + \frac{p_{0f}}{\alpha}, 1/8, \sqrt{y^2 + s(y)}\right) \right) \quad (34)$$

where $y = k_{0f}/\alpha$. Again we have used the antiparticle-particle symmetry property of the gap, $s(p_{0f}) = s(-p_{0f})$, to reduce the number of equations we need consider. Although the range of integration is infinite, the kernel of eqn (34) provides an effective cutoff Λ , where $\Lambda < 1$. Therefore we need only consider $s(\frac{p_{0f}}{\alpha})$ from $s(0)$ to $s(\Lambda)$ in doing numerical calculations. Λ is chosen in the same way as M ; namely at a point where $s(\Lambda)$ is sufficiently small so

that the contributions from $p_{0f} > \Lambda$ are negligible. Our $T \neq 0$ results and our $T = 0$ results are sufficient to provide all the information that we require.

We show the results of both our $T = 0$ and $T \neq 0$ calculations as functions of $\frac{p_{0f}}{\alpha}$ for $N=1$ in fig.6. One can see that the $T = 0$ curve joins smoothly on to the $T \neq 0$ solutions. One should observe that although we plot the $T \neq 0$ solutions as continuous curves, they are actually discrete points with $p_{0f} = \frac{2\pi}{\beta}(n + 1/2)$. As functions of $\frac{p_{0f}}{\alpha}$, these functions fall off rapidly for $\frac{p_{0f}}{\alpha} < 0.1$. This behaviour is roughly the same as was seen in momentum-dependent calculations [10], where for $0.02 < \frac{|\mathbf{p}|}{\alpha} < 0.1$ the solutions fell rapidly in $\frac{|\mathbf{p}|}{\alpha}$. It is this behaviour - the rapid fall in $s(\frac{p_{0f}}{\alpha})$ for $\frac{p_{0f}}{\alpha} < 0.1$ - which makes $\Sigma(T = 0, p_{0f} = 0)$ considerably smaller than $\Sigma(T = 0)_{const}$, our result from the previous section, as shown in fig.7. $\Sigma(T = 0, p_{0f} = 0)$ is roughly the same as $\Sigma(T = 0, \mathbf{p} = 0)$ in [10]. This suggests that the constant mass-gap approximation is not a good one, except as an order of magnitude calculation for the quantity r . In fig.8a we show the $m = 0$ mode of these solutions for various N as functions of $\frac{k_B T}{\alpha}$, and in fig.8b we show the $m = 0$ mode of these solutions for various $\frac{k_B T}{\alpha}$ as functions of N . One notices that the shape of the solutions in fig.8a is the same as that of the constant mass-gap solution (fig.4), which we have characterised as B.C.S -like. By looking at fig.8b one can see that as well as a critical temperature, T_c , there is also a critical number, N_c . N_c is the value of N above which $s = 0$ for all T and p_{0f} , and this can be found from fig.8b by locating the point where the gradient of the $T = 0$ curve tends to infinity. We only need consider the $m = 0$ mode at $T = 0$, since $s(m)$ is a monotonically decreasing function of both frequency and temperature. So if $s(T = 0, p_{0f} = 0) = 0$ this condition must be true for any T and p_{0f} . We find that N_c lies in the range $N_c \sim 1.8 - 2$. In fig.9 we show a N-T phase diagram, where we have included the value $N_c = 1.8$. Here we see that the phase boundary agrees qualitatively with that calculated in [10].

The existence of N_c leads us to the conclusion that any frequency or momentum dependence in the mass-gap equation induces a value of N_c . Our calculated value of N_c agrees well with [10], but [10] uses the instantaneous approximation and so has the incorrect $T \rightarrow 0$ limit. When compared with the correct $T \rightarrow 0$ limit of the 3-momentum -dependent mass-gap equation of [2], our value for N_c is smaller. (In [2] N_c was calculated to be 3.2). From

our results we are able to calculate a table of values for r , each at different values of N , as shown in table.1. These values are not much different from the value $r \sim 6$ calculated in section 2, but now there is a significant dependence of r on N ; the values of r are seen to fall with increasing N . The insensitivity of the r values to the introduction of a momentum dependence in the S-D equation was seen in [10], although for the instantaneous approximation; again this is roughly seen to be the case with the introduction of frequency dependence as shown by our results.

This completes our analysis of the frequency dependent solutions. In the next section we discuss ways of handling the transverse mode and other ways of extending our calculation.

5 Conclusion

As we have seen already in section 4 the constant mass-gap approximation is not a good one to make except possibly for the calculation of r , which is little changed by frequency dependence for the range of N -values considered here. Also we have seen that frequency dependence induces an N_c . Our result differs from [2], for we have been unable to introduce frequency and momentum dependence into our calculations while preserving a smooth $T \rightarrow 0$ limit, and also because we have no transverse contribution to the mass-gap equation. The reason why the introduction of momentum dependence is a hard problem at $T \neq 0$ is that three-dimensional Lorentz invariance is lost, since frequency dependence becomes discretized (in the imaginary time formalism). At $T = 0$ one can do the angular integration with full 3-momentum dependence, because one can exploit the three-dimensional symmetry. At $T \neq 0$ this is not possible, due to the preferred (frequency) direction; instead we are faced with an integral in 2-dimensional momentum space, exactly the integral which is discussed at the beginning of section 4.

Up to now in our analysis we have chosen not to discuss the transverse contribution, and have neglected it from our calculations due to the i-r divergence in its zeroth mode. It is important to stress that the i-r divergence is present only when $T \neq 0$. At $T = 0$, the effect of the transverse mode is merely to double the number of flavours, so giving us an N_c in the range 3.8 – 4. To treat the i-r divergence at $T \neq 0$ one needs to regulate the

integral in eqn (20). A reasonable way to do this might be to introduce massive fermion propagators into our calculation of $\Pi_{\mu\nu}$, the mass of the fermion propagators being calculated self consistently in eqn (19). A major problem with this refinement would be the requirement of self consistency in our calculation of the photon propagator when we have any frequency or momentum dependence in the fermion mass. Nevertheless, it might be worth considering the simpler problem of a constant mass in this sort of calculation; this may not give us reliable values of $\Sigma(T = 0)$ and $k_B T_c$, but the value of r it gives might not change very much if frequency or momentum dependence were to be included. To tackle the harder problem of including frequency or momentum dependence in this extension to our work, we may be forced either to consider our calculation of $\Pi_{\mu\nu}$ as a separate integral equation, so that the calculations would involve two integral equations coupled together, not one; or we may have to use an ansatz for our expected form of the fermion mass.

As well as the above extension to our work involving the transverse contributions, another important step will be to introduce momentum dependence. Although we have stated that this is difficult due to the computational complexity, one may be able to approximate the kernel in such a way as to simplify the problem. One of the major goals in this series of numerical calculations for $T \neq 0$ should be to join on with the results of [2] in a smooth $T \rightarrow 0$ limit, and this necessitates a successful treatment of momentum dependence.

As to the question of QED_3 as a model of superconductivity in the context of our calculations, consider the case $N = 1$. If we crudely double the number of flavours so as to account for the transverse mode, this will effectively count as $N = 2$ which is the value required for QED_3 in a model of high T_c superconductivity [13]. We find that $k_B T_c \sim 10^{-3} \alpha$ in agreement with [10], once rescaled to agree with [2] as regards N_c . As pointed out in [10] this gives a value of α of the order of $8eV$ for $T_c \sim 100^\circ K$. As stated in [10] this is still much higher than the typical Heisenberg exchange energies, but might be acceptable by suitable rescaling of the fermion lattice operators in the lattice model of [13]. It is interesting to note as a concluding remark that our suggested way to treat the i-r divergence in the zeroth mode of the transverse contribution may effectively reduce α by an order of magnitude or more, so on this basis alone it is a calculation worth considering.

Acknowledgements

D.J.Lee is very grateful to his supervisor I.J.R.Aitchison for useful discussions, and for the editing of the manuscript. He would also like to thank G.Metikas for his diligent proof reading of various formulae given in this paper. The support of a Research Studentship from PPARC(UK) is acknowledged.

References

- [1] R.D Pisarki, *Phys. Rev.* **D29** (1984) 2423.
- [2] T.W Appelquist, M.Bowick, D.Karabali and L.C.R Wijewardhana, *Phys. Rev.* **D33** (1986) 3704.
T.W Appelquist,D.Nash and L.C.R Wijewardhana *Phys. Lett.* **60** (1988) 2575.
- [3] M.R Pennington and D.Walsh, *Phys. Lett* **B253** (1991) 246.
- [4] E.Dagotto, A.Kocic and J.B Kogut, *Phys. Rev. Lett.* **62** (1989) 1083 and *Nucl. Phys.* **B334** (1990) 279.
- [5] D.Nash,*Phys. Rev. Lett.* **62** (1989) 3024.
- [6] D.Atkinson, P.W Johnson and P.Maris ,*Phys. Rev.* **D42** (1990) 602.
- [7] P.Maris,*Phys.Rev.***D54** (1996) 4049.
- [8] K.-I.Kondo,preprint OUTP-96-50P,CHIBA-EP-96;hep-th/9608402.
- [9] N.Dorey and N.E.Mavromatos,*Phys.Lett.***B266** (1991) 163.
- [10] I.J.R Aitchison, N.Dorey, M.Klein-Kreisler and N.E Mavromatos, *Phys. Lett.* **B294** (1992) 91.
- [11] I.J.R Aitchison and M.Klein-Kreisler, *Phys. Rev.* **D50** (1993) 1068.
- [12] I.J.R Aitchison,*Z.Phys.* **C67** (1995) 303.

- [13] N.Dorey and N.E Mavromatos, *Nucl. Phys.* **B386** (1992) 614.
- [14] A.Kovner and B.Rosenstein, *Phys. Rev.* **B42** (1990) 4748.
A.Dorey and N.E Mavromatos, *Phys. Lett.* **B250** (1990) 107.
G.W Semenoff and N.Weiss, *Phys. Lett.* **B250** (1990) 117.

Figure Captions

Figure 1. Contributions to $\Delta_{\mu\nu}$ to leading order in $1/N$

Figure 2 (a). Π_1 as a function of explicit m and 3-momenta, p_b .

Figure 2 (b). Π_2 as a function of explicit m and 3-momenta, p_b .

Figure 2 (c). Π_3 as a function of explicit m and 3-momenta, p_b

Figure 3 (a). Top graph: The numerical data points and the approximation $\beta p_b/8$ for the $m \neq 0$ modes of $\Pi_1(m = 1, p_b)$, shown for $p_b\beta$ ranging from 0 – 4. Bottom graph: The numerical data points and the approximation $\beta p_b/8$ for the $m \neq 0$ modes of $\Pi_1(m = 1, p_b)$, shown for $p_b\beta$ ranging from 0 – 36.

Figure 3 (b). Top graph: The numerical data points and the approximation $\beta p_b/8$ for the $m \neq 0$ modes of $\Pi_3(m = 1, p_b)$, shown for $p_b\beta$ ranging from 0 – 9. Bottom graph: The numerical data points and the approximation $\beta p_b/8$ for the $m \neq 0$ modes of $\Pi_3(m = 1, p_b)$, shown for $p_b\beta$ ranging from 0 – 36.

Figure 4. The numerical results for the constant mass calculation as functions of $\frac{T}{k_B\alpha}$ for $N = 0.5, 1, 1.5$.

Figure 5. Plot of $k_B T_c/\alpha$ vs. N for the constant mass calculation; the points are the numerical values calculated from (21), the curve is an approximate form for $T_c(N)$ as given by equation (28).

Figure 6. The numerical results for the frequency dependent solution, $\Sigma(p_{0f}, T)$ as a function of p_{0f} for various $k_B T/\alpha$ at $N = 1$.

Figure 7. A comparison of Σ_{const} , the mass for the constant mass calculation, with $\Sigma_{freq}(m = 0, T = 0)$, the zero-frequency mass for the frequency dependent calculation, as functions of N .

Figure 8 (a). The numerical results for the frequency dependent mass calculation as functions of $\frac{T}{k_B\alpha}$ for $N = 0.5, 0.7, 1$.

Figure 8 (b). The numerical results for the frequency dependent mass calculation as functions of N for $Tk_B/\alpha = 0, 0.001, 0.002, 0.004$, used to estimate N_c in the case of $Tk_B/\alpha = 0$.

Figure 9. A phase diagram for the frequency dependent solution, showing the boundary between the massless and massive fermion phases in the $N - T$ plane.

Table Captions

Table 1. The values of r calculated for various N in the frequency dependent mass calculation.

$$\text{wavy line with a dot} = \text{wavy line} + \text{wavy line with a circle} + \text{wavy line with two circles} + \dots$$

Fig. 1

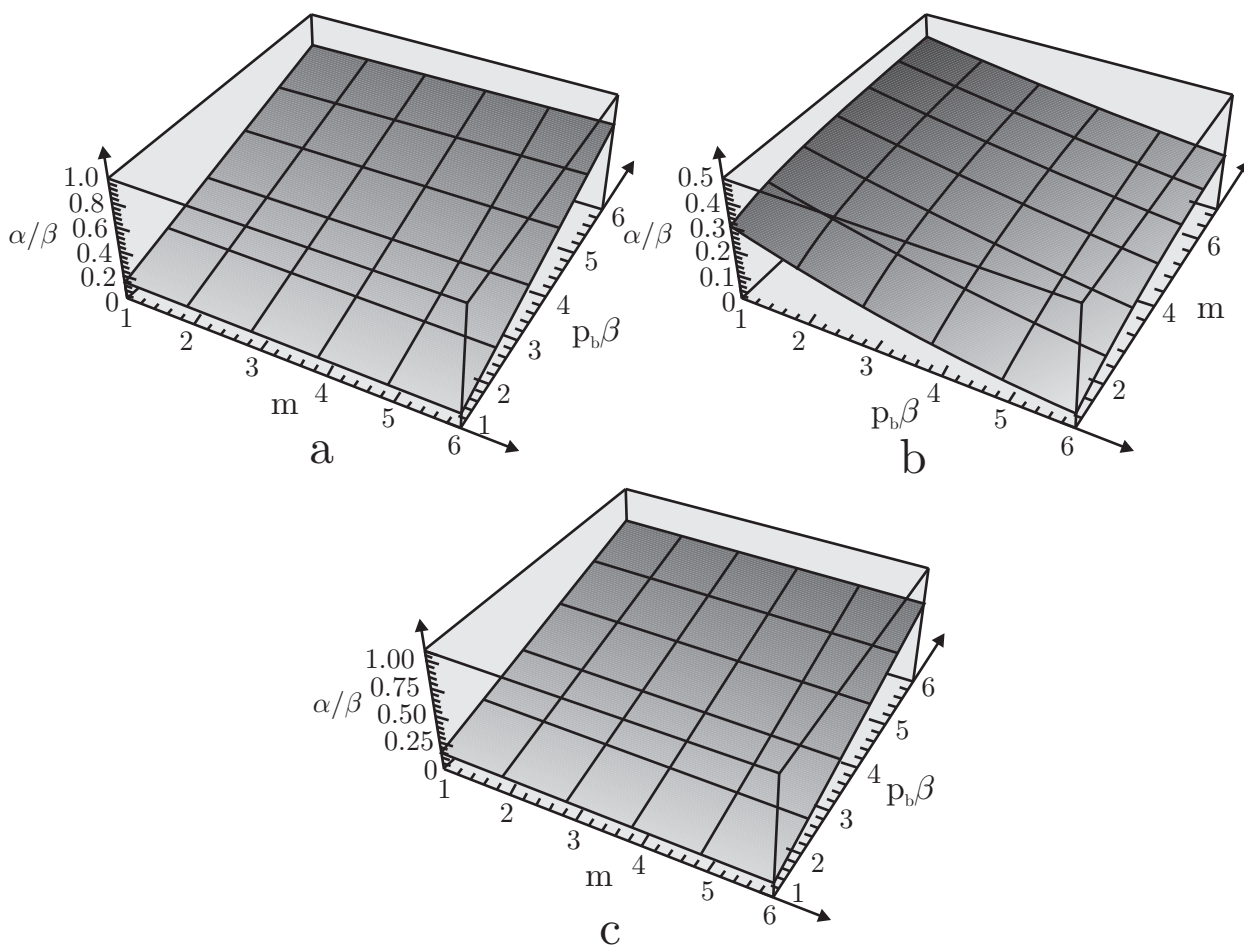


Fig. 2

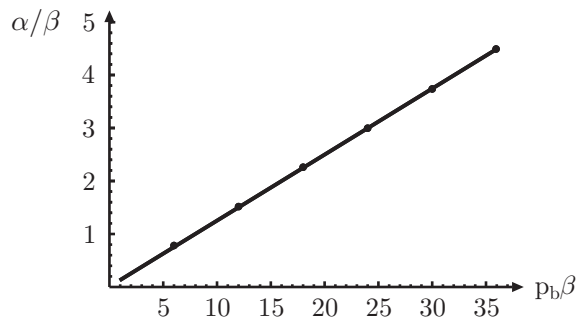
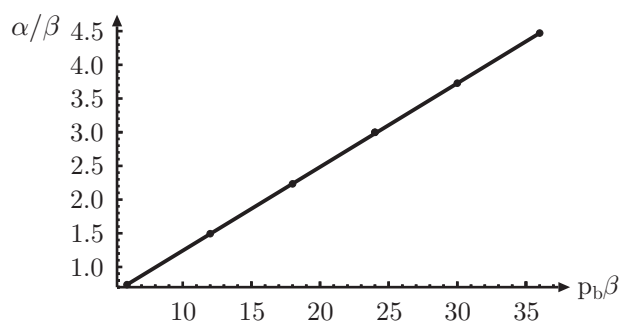
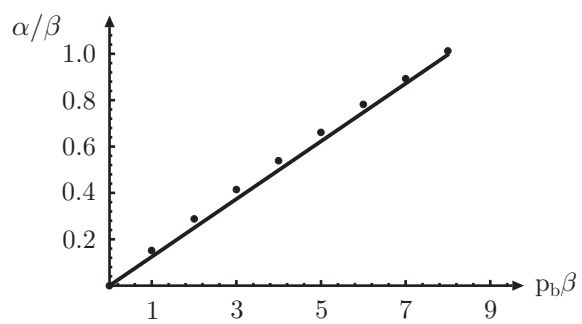
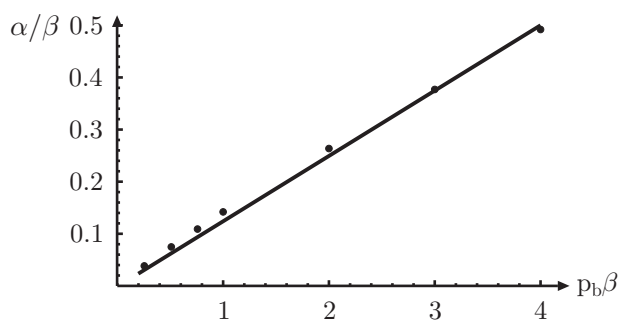


Fig. 3a

Fig. 3b

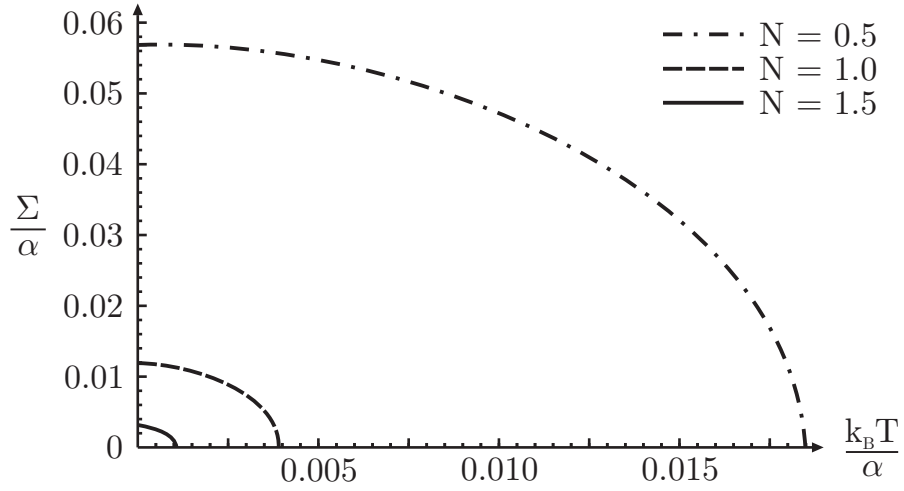


Fig. 4

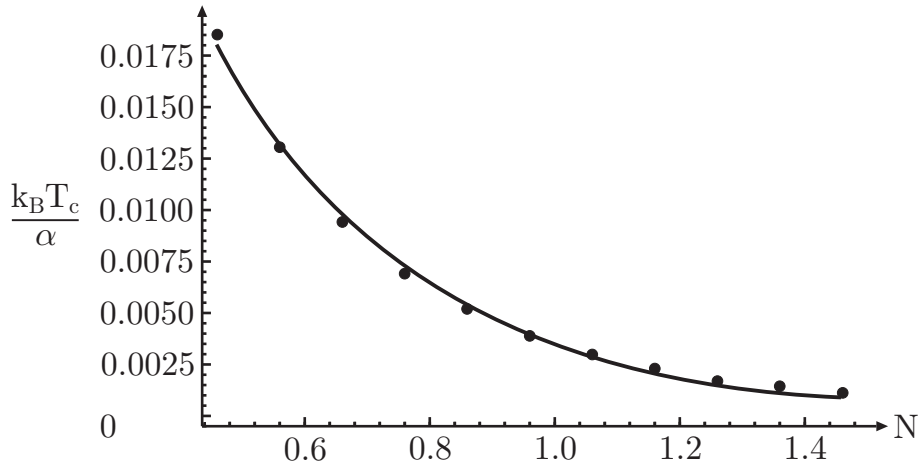


Fig. 5

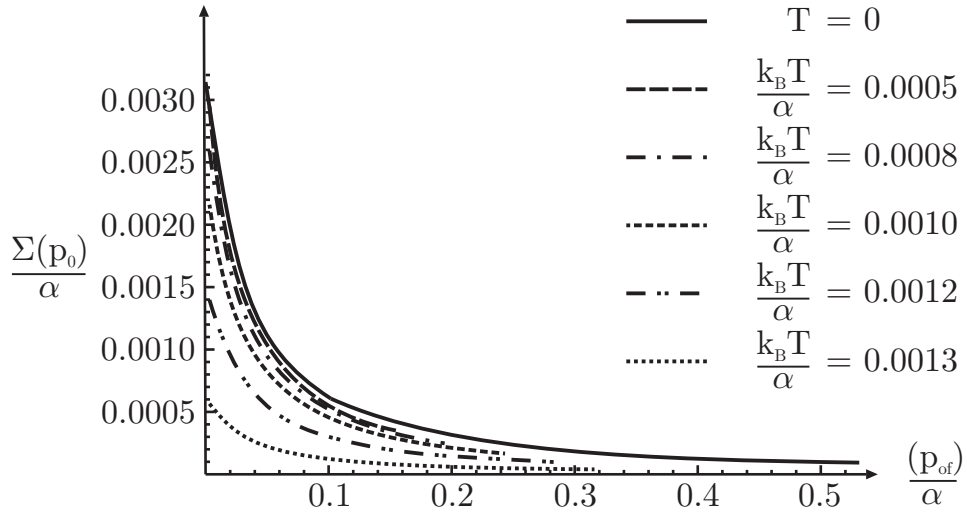


Fig. 6

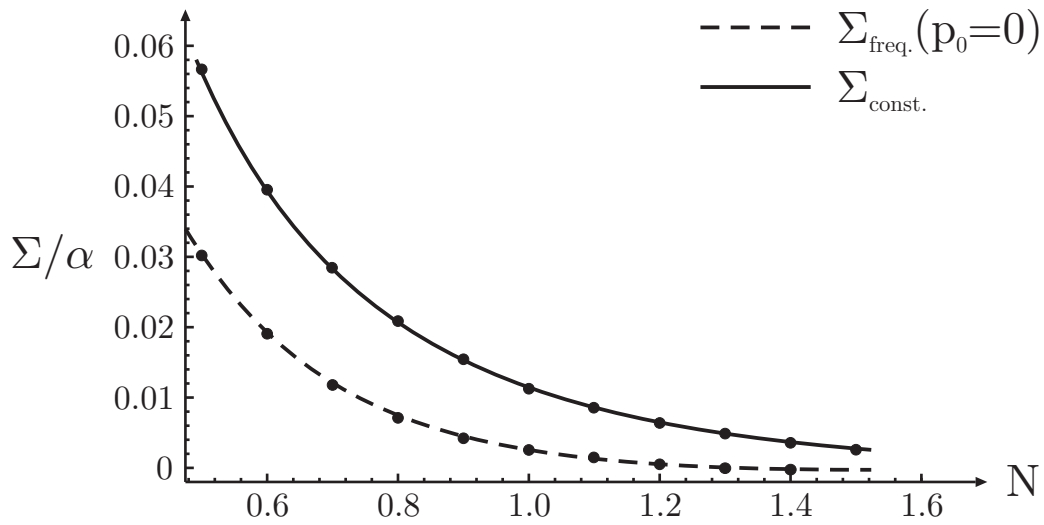


Fig. 7

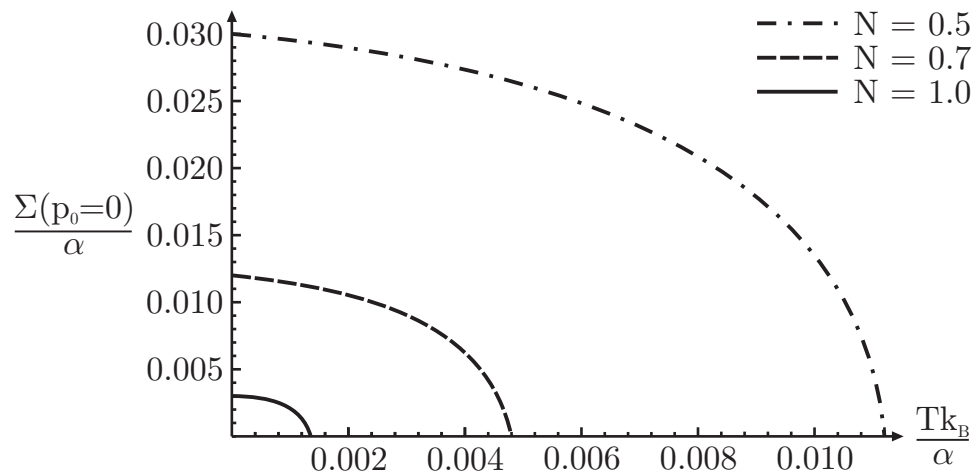


Fig. 8a

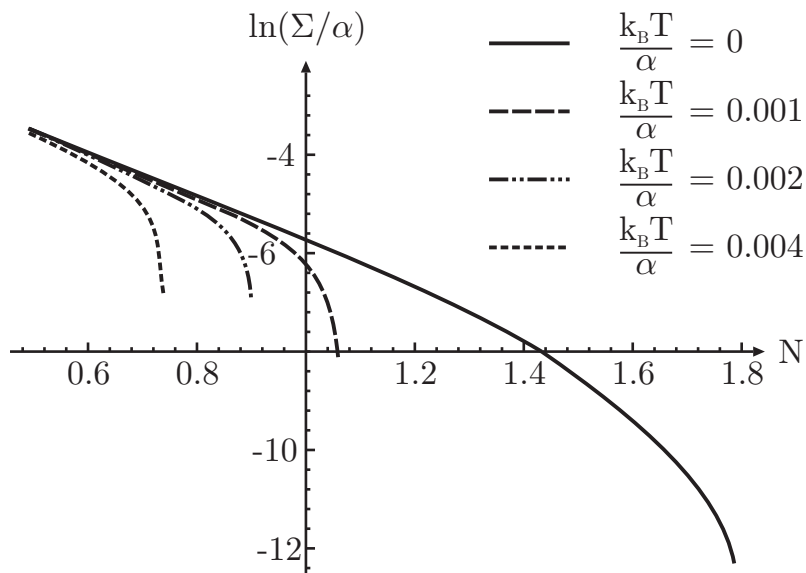


Fig. 8b

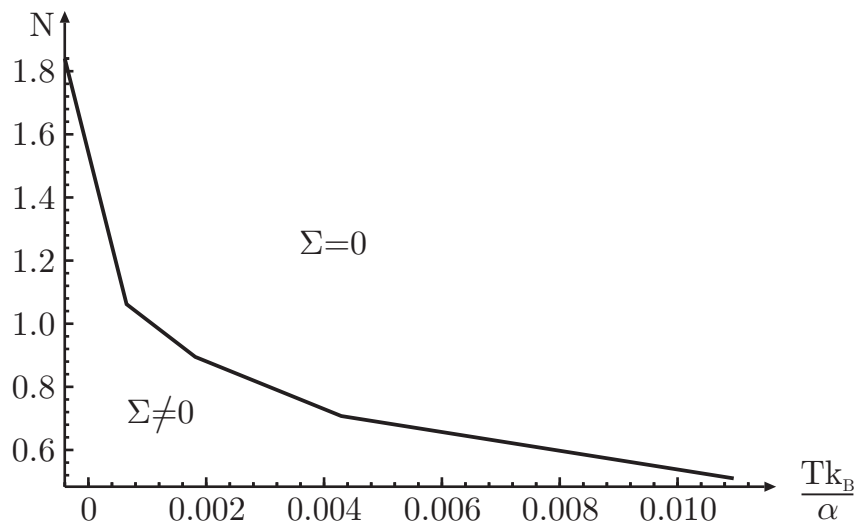


Fig. 9